

# Imaging Constitutive Exocytosis with Total Internal Reflection Fluorescence Microscopy<sup>Ⓞ</sup>

Jan Schmoranzler,\* Mark Goulian,\* Dan Axelrod,† and Sanford M. Simon\*

\*Laboratory of Cellular Biophysics, The Rockefeller University, New York, New York 10021; and †Department of Biophysics, University of Michigan, Ann Arbor, Michigan 48109-1055

**Abstract.** Total internal reflection fluorescence microscopy has been applied to image the final stage of constitutive exocytosis, which is the fusion of single post-Golgi carriers with the plasma membrane. The use of a membrane protein tagged with green fluorescent protein allowed the kinetics of fusion to be followed with a time resolution of 30 frames/s. Quantitative analysis allowed carriers undergoing fusion to be easily distinguished from carriers moving perpendicularly to the plasma membrane. The flattening of the carriers into the plasma membrane is seen as a simultaneous rise in

the total, peak, and width of the fluorescence intensity. The duration of this flattening process depends on the size of the carriers, distinguishing small spherical from large tubular carriers. The spread of the membrane protein into the plasma membrane upon fusion is diffusive. Mapping many fusion sites of a single cell reveals that there are no preferred sites for constitutive exocytosis in this system.

**Key words:** membrane fusion • constitutive secretion • green fluorescent protein • vesicle • evanescent wave

## Introduction

The final stage of secretion is fusion of a transport vesicle with the plasma membrane. Most of the data in support of this model come from assays on individual fusion events in regulated exocytosis. When a cell is stimulated to secrete, contents are simultaneously released in large quanta. This was originally detected by the arrival of quantal packets of synaptic transmitter at the postsynaptic cell (Fatt and Katz, 1952). The quantal release of vesicular contents upon stimulation also has been observed with amperometry (Zhou and Misler, 1995; Albillos et al., 1997), epifluorescence microscopy (Ryan et al., 1997), and total internal reflection fluorescence microscopy (TIR-FM)<sup>1</sup> (Lang et al., 1997). The fusion of individual vesicle membranes has been examined by the measurement of jumps in membrane capacitance (membrane surface area) during stimulated secretion in chromaffin cells (Neher and Marty, 1982). The kinetics of the initial steps of fusion were re-

solved by assaying the opening of single fusion pores during stimulated secretion in mast cells (Fernandez et al., 1984; Zimmerberg et al., 1987), neutrophils (Nusse and Lindau, 1988; Gillis et al., 1991), and viral-mediated fusion (Zimmerberg et al., 1994).

Constitutive secretion, the process that delivers newly synthesized proteins to the plasma membrane and external media, occurs in all eukaryotic cells. It is generally accepted that constitutive secretion uses a similar mechanism to that of regulated secretion (Palade, 1975). They share many homologous biochemical components, including the SNAPs and SNAREs (Rothman and Wieland, 1996). The inability to trigger constitutive exocytosis, however, has made it difficult to address some of the mechanistic issues. In the absence of a trigger, it has been difficult to assay fusion of single vesicles during constitutive exocytosis. While it is accepted that transport is via a membrane-enclosed carrier, it remains to be resolved whether these carriers are tubular or spherical. Previously, laser scanning confocal microscopy and wide-field epifluorescence microscopy have been used to demonstrate that the rate of secretion from the constitutive secretory pathway follows simple first order kinetics (Hirschberg et al., 1998). However, a higher temporal resolution and higher signal-to-background ratio are required to resolve the detailed kinetics of individual exocytic events.

<sup>Ⓞ</sup>The online version of this article contains supplemental material.

Address correspondence to Sanford M. Simon, Laboratory of Cellular Biophysics, The Rockefeller University, 1230 York Avenue, New York, NY 10021. Tel.: (212) 327-8130. Fax: (212) 327-8022. E-mail: simon@rockvax.rockefeller.edu

<sup>1</sup>Abbreviations used in this paper: GFP, green fluorescent protein; TIR-FM, total internal reflection fluorescence microscopy; VSVG, vesicular stomatitis virus glycoprotein.

In this study, we used TIR-FM to acquire high resolution video rate images of the fusion of single constitutive secretory carriers with the plasma membrane. Over the past decade, TIR-FM (for review see Axelrod et al., 1992) has been used to image a variety of surface events, such as polymer movement near an interface (Migler and Hervet, 1993), single molecule interactions in vitro (Funatsu et al., 1995), and the dynamics of cellular membranes in vivo (Steyer et al., 1997; Oheim et al., 1998). In TIR-FM, an excitatory laser beam is directed through the coverslip at an angle steep enough that it completely reflects off the water-coverslip interface. This results in what is often called an evanescent field, which is a field that decays exponentially with distance into the aqueous medium. The characteristic decay distance depends on the incident angle. For the experiments described in this paper, there is an excitation layer extending  $\sim 70$  nm from the microscope coverslip. As a result, only fluorescent molecules within this distance from the coverslip are excited, enabling high signal-to-background imaging of surface events.

TIR-FM has been used to image the release of soluble vesicular contents during regulated exocytosis (Steyer et al., 1997). However, the contents diffuse away quickly, making analysis difficult. To be able to quantitatively analyze constitutive exocytosis, we made two modifications to improve the resolution. First, we used a high numerical aperture lens to perform prismless TIR-FM on living cells (Axelrod, 1989; Steyer et al., 1997). In contrast to the traditional approach of using a prism to couple the exciting beam at a supercritical angle to the interface, a high numerical aperture lens (NA 1.65) is used to deliver the exciting beam, which results in a substantial increase in light collection. Second, we examined the delivery of a membrane protein to the plasma membrane rather than the luminal contents of a secretory vesicle. A membrane protein should diffuse considerably more slowly than a released soluble fluorophore. The combination of these two modifications allowed us to examine the kinetics of vesicle fusion and subsequent diffusion of membrane proteins into the plasma membrane.

The reporter used in this study is the thermoreversible folding mutant ts045 vesicular stomatitis virus glycoprotein (VSVG; Wehland et al., 1982), with the green fluorescence protein (GFP) fused to its cytoplasmic tail (VSVG-GFP), which has been described elsewhere (Presley et al., 1997; Toomre et al., 1999). This mutant is retained in a misfolded form in the ER at 40°C, but upon shifting to 33–35°C, moves synchronously to the Golgi complex, from where it is transported to the plasma membrane. In this study, VSVG-GFP was transiently expressed in COS cells, and its delivery to the plasma membrane was imaged shortly after shifting to 33–35°C.

Single post-Golgi carriers of various morphologies were followed as they approached the plasma membrane, and the spread of their membrane cargo (VSVG-GFP) upon fusion was quantified. The analysis revealed a diversity of fusion kinetics for post-Golgi carriers and allowed us to measure the diffusion constant for the spread of VSVG-GFP into the plasma membrane. The data support the proposal that long tubular structures contribute to the transport from the Golgi complex to the cell surface (Hirschberg et al., 1998; Toomre et al., 1999). Mapping the coordi-

nates of fusion sites for a single secreting cell indicates constitutive exocytosis occurs randomly across the surface.

## Materials and Methods

### TIR-FM Setup

The prismless TIR-FM was used as described previously (Axelrod, 1989). It consists of an inverted epifluorescence microscope (model IX-70; Olympus America Inc.) equipped with a high numerical aperture lens (Apo 100X NA 1.65, Olympus). To align the TIR-FM, the widened and collimated beam from an argon ion laser (model 543-AP A01; Omnicrome) was attenuated with neutral density filters, cropped by a diaphragm, and reflected off two mirrors to the dichroic mirror of the microscope. A convex lens ( $f = 20$  cm) in the beam path was used to focus the laser beam onto the back focal plane of the objective. Two mirrors were tilted to change the incident angle of the laser beam onto the TIR interface.

### Estimation of the Evanescent Field Decay Length

A right angle prism (hypotenuse facing up) was coupled with immersion liquid ( $n = 1.78$ ) onto the sample side of the coverslip. Since the refractive index of the prism ( $n = 1.55$ ) is too high, relative to the coverslip, to enable TIR at this incident angle, the laser beam propagated through the prism onto a vertical screen beside the setup. The incident angle was determined by applying Snell's law, and the decay length was calculated from the incident angle (Axelrod, 1989). The incident angles used in our experiments were estimated to range between 63° and 54°, which is significantly above the critical angle of 51°, and results in an evanescent field with a decay length between 90 and 50 nm.

### Tissue Culture and Transfection

COS-1 cells (African green monkey; American Type Culture Collection) were maintained in DME (Sigma Chemical Co.) with 10% FBS at 37°C in a 5% CO<sub>2</sub> incubator. Cells were plated on acetone-cleaned coverslips, which had a refractive index of 1.78 (Olympus America Inc.), and had been coated with fibronectin (Life Technologies) to promote cell adherence. Cells were transiently transfected with the plasmid VSVG-GFP ts045 (Presley et al., 1997) using FuGENE™ 6 (Boehringer Mannheim) according to the manufacturer's protocol. At 12 h after transfection, cells were shifted from 37° to 40°C for 36 h to accumulate the VSVG-GFP in the ER. Cells were imaged in modified MEM without phenol red (Sigma Chemical Co.) with 10% FBS at 33–35°C. The temperature was maintained by a homebuilt incubator consisting of a thermally insulating hood covering the whole microscope and an air-stream incubator (Air Therm; World Precision Instruments), which is similar to the setup described in Inouye and Spring (1997).

### Image Acquisition and Analysis

Samples were excited with the 488-nm line of an argon laser. The dichroic mirror (D460/40×) and the emission band pass filter (model HQ525/50M; Chroma Technologies Corp.) were used. Images were acquired with a 12-bit-cooled CCD (Orca I, model C4742-95; Hamamatsu) with a pixel size of 6.7  $\mu\text{m} \times 6.7 \mu\text{m}$ , an image acquisition card (NI-IMAQ 1424), and controlled by in-house software written in LABVIEW™5.1 using the IMAQ Vision package (all three from National Instruments). The maximum speed of image acquisition was either 30 frames/s ( $4 \times 4$  binning) or 18 frames/s ( $2 \times 2$  binning). Images containing a region of interest of the cell were streamed to memory on a PC during acquisition and saved to a disk.

Image analysis to obtain the total intensity, the peak intensity, and the width of the carrier was performed with in-house software written in LABVIEW™5.1 using the IMAQ Vision package. For analysis of single fusion events, each acquired sequence (1,000–2,000 frames) was reviewed multiple times on screen at various settings of the intensity look-up table to pick out all visible events. The coordinates for each fusion event were determined by identifying the local maximum of fluorescence intensity. Only a small region of interest around each fusion site was used for further analysis. These were selected such that they were both large enough to yield a good Gaussian fit of the carrier fluorescence, and small enough to prevent the influence of other fluorescent particles on the analysis.

All fusion sequences were analyzed in the following manner. The center of mass of the carrier was tracked for the entire sequence. The radial

intensity distribution  $I(r)$  of the carriers was fit for each frame with a non-linear Levenberg-Marquardt routine to the Gaussian:  $I(r) = I_0 \exp(-r^2/w^2) + BG$ , where  $r$  is the distance of each pixel to the center of mass. The fitting parameters are  $I_0$ ,  $w$ , and  $BG$ , where  $I_0$  is the peak intensity,  $BG$  is the background intensity, and  $w$  is the measure of the width (the Gauss width). The total intensity of the vesicle was computed by integrating the background-subtracted intensity over the entire region of interest. The fusion start was defined as the frame at which the second derivative of the smoothed total intensity was maximal. The rise time of the total intensity was the time difference between the fusion start and the frame where the smoothed total intensity reached its maximum within 5%. The diffusion constant was calculated by taking the carrier at the fusion start to be an instantaneous point source for diffusive material (Crank, 1995). The intensity profile as a function of time is given by:

$$I(r,t) = \frac{I_0}{4\pi Dt} \exp\left(-\frac{r^2}{4Dt}\right).$$

The square of the width of this Gaussian,  $4Dt$ , is linear over time  $t$ , with the slope proportional to the diffusion constant  $D$ .

### Calculation of the Ratio $TI_{flat}/TI_{spherical}$

The total fluorescence intensities for a flattened ( $TI_{flat}$ ) and spherical ( $TI_{spherical}$ ) vesicle are directly proportional to the excitation intensity of the evanescent field  $I(z)$ , which decays exponentially from the coverslip into the cell:  $I(z) = I_0 \exp(-z/d)$ . Here,  $z$  is the distance from the coverslip,  $I_0$  is the intensity in the plane at  $z = 0$ , and  $d$  is the decay length of the evanescent field. The total intensities for the flat and spherical configurations are calculated by integrating the excitation field  $I(z)$  over a circular disk and sphere, respectively:

$$TI_{flat} = cI_0(4\pi R^2) \quad TI_{spherical} = c2\pi R \int_0^{2R} dz I_0 \exp(-z/d),$$

where  $R$  is the radius of the vesicle.

The constant  $c$  depends on the quantum yield and extinction coefficient of the fluorophore and the collection efficiency of the lens. After evaluating the integral and taking the ratio we find the following:

$$\frac{TI_{flat}}{TI_{spherical}} = \frac{2R}{d} \frac{1}{1 - \exp(-2R/d)}.$$

### Thresholded Image of VSVG-GFP in the Plasma Membrane

The highly thresholded image shown in Fig. 5 was created by averaging the first frame of each image sequence ( $n = 30$ ), followed by subsequent nearest neighbor averaging (with all eight neighbors). The threshold was chosen to show bits between 1 (black) and 5 (bright gray) on a 256-bit scale.

### Online Supplemental Material

**Description of Supplementary Figures:** Both plots are supplementary information to the data shown in Table II. For detailed description of the parameters used see Materials and Methods. All supplementary materials are available at <http://www.jcb.org/cgi/content/full/149/1/23/DC1>.

**Figure 1.** Total delivered intensity over the rise time. The total fluorescence intensity (maximum intensity reached shortly after fusion start) delivered by 45 carriers, which fused with the plasma membrane, is plotted as a function of their rise time (the time in which the carriers are flattening down into the plasma membrane while delivering all their membrane cargo). The linear fit to the data (shown in red) suggests that a longer rise time is directly correlated to a larger membrane cargo.

**Figure 2.** Total delivered intensity over the intensity of the carrier before fusion. The total fluorescence intensity (maximum intensity reached shortly after fusion start) delivered by 45 carriers, which fused with the plasma membrane, is plotted as a function of the fluorescence intensity just before fusion. The linear fit to the data (shown in red) suggests that these carriers with a smaller initial fluorescence seem to deliver less total membrane cargo.

**Description of Supplementary Video Material.** All video sequences show post-Golgi carriers in COS-1 cells transfected with ts 045 VSVG-GFP as a constitutively secreted membrane protein. The sequences are taken ~30–50 min after the release of the temperature block in the ER in TIR-FM.

**Video 1: View of Many Carriers.** The sequence, taken at 30 frames/s, shows a part of the cell surface imaged in TIR-FM. The cell edge is in the upper left, the Golgi is in the lower right corner (pixel size, 256 nm). There are three types of behaviors of the post-Golgi carriers: (1) carriers that are stationary; (2) carriers that are moving, but not fusing; and (3) carriers that fuse to the plasma membrane. As can be seen on the extreme left and right, fusion occurs with a bright local burst of fluorescence followed by a spread of the fluorescence. The carrier on the extreme left was observed doing transport, docking, and fusion during the acquisition time. The two carriers on the extreme right did not move significantly before they fused.

**Video 2: Small Carrier Fusion.** This sequence (Fig. 2, b and c), taken at 30 frames/s, shows a highly enlarged region of interest containing a small dotlike carrier (pixel size, 256 nm) undergoing fusion with the plasma membrane. The fusion can be seen as a local increase followed by a spread of the fluorescence intensity due to diffusion of the VSVG-GFP in the plasma membrane.

**Video 3: Large Tubular Carrier Fusion.** This sequence (10 frames/s; pixel size, 134 nm) shows an enlarged region of interest containing a large tubular carrier undergoing transport, docking, and fusion (see selected frames in Fig. 3 and quantification in Fig. 4 A). During the transport, the intensity of the tubule is changing slightly, which is probably due to movement in the vertical direction, in and out of the evanescent field. Just before fusion the tubule seems to round up to a dot. Fusion occurs with a huge burst of fluorescence followed by a spread of the fluorescence.

## Results and Discussion

To observe constitutive exocytosis, we examined the delivery of an integral membrane protein, VSVG-GFP, into the plasma membrane. Studying delivery of a membrane protein offered a number of advantages over delivery of a luminal marker. First, assaying release of luminal markers has been limited by temporal resolution: upon fusion luminal contents diffuse away quickly, often in less than one image frame (Steyer et al., 1997; Oheim et al., 1998). GFP-labeled membrane proteins should move away from the site of fusion more slowly, both because of their greater size and because they have to diffuse within the plasma membrane. This should allow us to examine the kinetics of exocytosis in greater detail. Second, the concentration of membrane-permeant luminal fluorophores, such as acridine orange, is sensitive to changes in the vesicle lumen. In our experiments, the concentration of the fluorophores remains constant in each carrier since the GFP is synthesized as part of a membrane protein. Third, the fluorescence of luminal fluorophores is sensitive to physiological changes inside the vesicle, such as pH. The GFP fluorophores in our experiments were synthesized on the cytoplasmic side of the VSVG and, therefore, were unaffected by changes inside the vesicles. Finally, by quantitatively demonstrating that the fluorescence of a membrane-bound GFP in a carrier is delivered to the plasma membrane, we could ensure that we were monitoring fusion of the carrier and not lysis or movement out of the plane of focus.

A cell transfected with VSVG-GFP was imaged with both epifluorescence microscopy and TIR-FM (Fig. 1). Under epifluorescence microscopy, the entire cell was visible, with a particularly strong signal in what is probably the Golgi complex (Fig. 1 A, bright spots on the left side). In TIR-FM, the excitatory evanescent field decays exponentially from the coverslip over ~70 nm (see Materials and Methods). The Golgi complex was not visible, indicating that it was far enough away from the coverslip to be outside the evanescent field (Fig. 1 B). Instead, discrete particles were observed that exhibited various morphologies, ranging from small spheres to tubular structures that

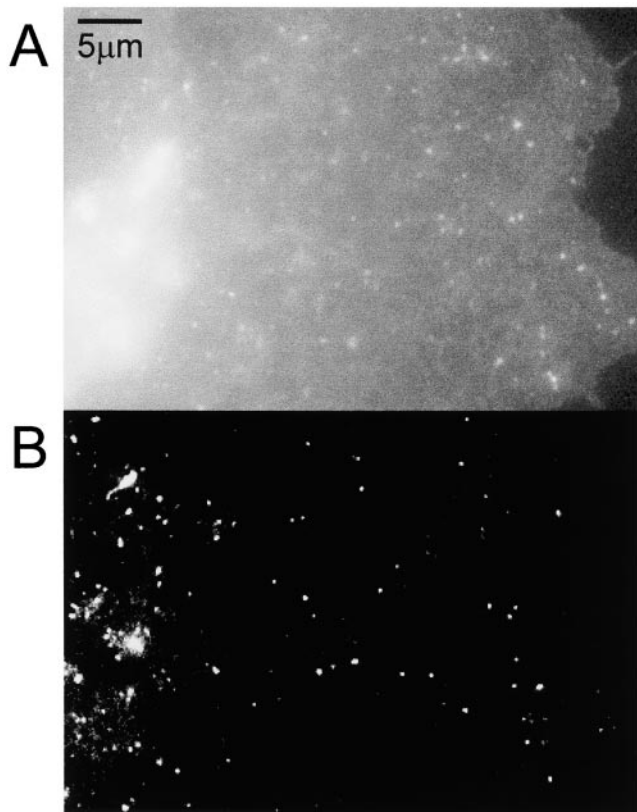


**Figure 1.** Comparison of epi- and TIR illumination. A COS cell transfected with VSVG-GFP was imaged using (A) epi- and (B) TIR illumination.

can be up to many microns long (Hirschberg et al., 1998; Toomre et al., 1999). In this paper, we refer to these as carriers, independent of their morphology.

Each of the carriers was characterized by its movement, total intensity, peak intensity, and the width of its intensity profile (cells were imaged at 30 frames/s). Changes of the fluorescence intensity were the consequence of the fluorescent cargo moving relative to the coverslip, thereby changing the excitation by the evanescent field. The carriers that we imaged fell into three groups. Some carriers stopped moving and remained stationary adjacent to the membrane (or were stationary during the entire observation period). These are carriers that we believe docked, but did not fuse, during the 1-min observation period.

The second group of carriers showed synchronous increases and decreases in the total and peak intensities with no significant change in the width (Fig. 2, A and C). We believe that these carriers moved in and out of the plane of the evanescent field without fusing with the membrane. In conventional epifluorescence the observed width of a fluorescent object widens as it moves out of the plane of focus, which was not observed with these carriers. This is the consequence of the narrow depth of the evanescent field in TIR-FM (50–90 nm), which is significantly smaller than the depth of field of the objective. Thus, the fluorophores are never excited outside of the plane of focus.

The third group showed a synchronous increase in the total, peak and width of the fluorescence (Fig. 2, B and D).

If a carrier fuses with the plasma membrane, the total intensity should increase as the vesicle flattens to the membrane (moving the fluorophores into the evanescent field), whereas the peak intensity should transiently increase and then decrease as VSVG-GFP diffuses laterally into the membrane. In addition, the width will increase as a result of this diffusion. Therefore, we believe these carriers have fused to the plasma membrane. (Examples of carriers from each of these groups can be seen in Video 1 at <http://www.jcb.org/cgi/content/full/149/1/23/DC1>.)

Selected temporal frames are shown for a carrier that fused to the membrane (Fig. 2 D and Video 2 at <http://www.jcb.org/cgi/content/full/149/1/23/DC1>). The total intensity, peak intensity, and the width squared of the fluorescence for this fusion event are plotted as a function of time (Fig. 2 B). These data allow us to clearly distinguish three temporal phases, which we label stationary, rise, and spread (Table I). During all three phases, the center of mass of the carrier was tracked to account for lateral movements, which were on average less than one pixel per frame.

### **Stationary Phase**

During this phase, the total intensity, the peak intensity, and the width were constant. The fact that the total and peak intensities were constant suggests there was no detectable movement of the carrier perpendicular to the evanescent field. Further, the fact that the width remained constant indicates that the VSVG-GFP was not spreading into the plasma membrane. Therefore, the stationary phase probably represents a vesicle that was docked or tethered close to the plasma membrane. Occasionally, a slight increase in the total and peak intensities was evident just before the rise phase (data not shown). This may correspond to a movement of the carrier towards the plasma membrane before fusion.

### **Rise Phase**

During the second phase, the total and peak intensities rose rapidly and the width squared began to increase in a roughly linear fashion (Fig. 2 B). Importantly, the increase in all three values was simultaneous for all analyzed fusion events ( $n > 100$ ). The increase in width indicates that the VSVG-GFP was diffusing into the plane of the plasma membrane. The increase of total fluorescence (average of  $4.6 \pm 2.0$ -fold;  $n = 16$ ) implies that the fluorescent cargo was moving towards the coverslip, where the evanescent field was greatest. This increase in the total intensity is expected when a spherical vesicle containing a membrane marker flattens down into the plasma membrane (Table I). Since the evanescent field decays exponentially with distance into the cell, the total intensity of a stationary spherical vesicle ( $TI_{spherical}$ ) at the plasma membrane must be lower than the total intensity of the same vesicle after flattening down into the plasma membrane ( $TI_{flat}$ ). In the latter case it forms a disk in the plane of the plasma membrane with an area identical to the surface of the vesicle. The magnitude of this intensity increase can be described by the ratio  $TI_{flat}/TI_{spherical}$ , which is independent of the position of the plasma membrane in the evanescent field. For a 250-nm-diam spherical vesicle with the fluorophore uni-

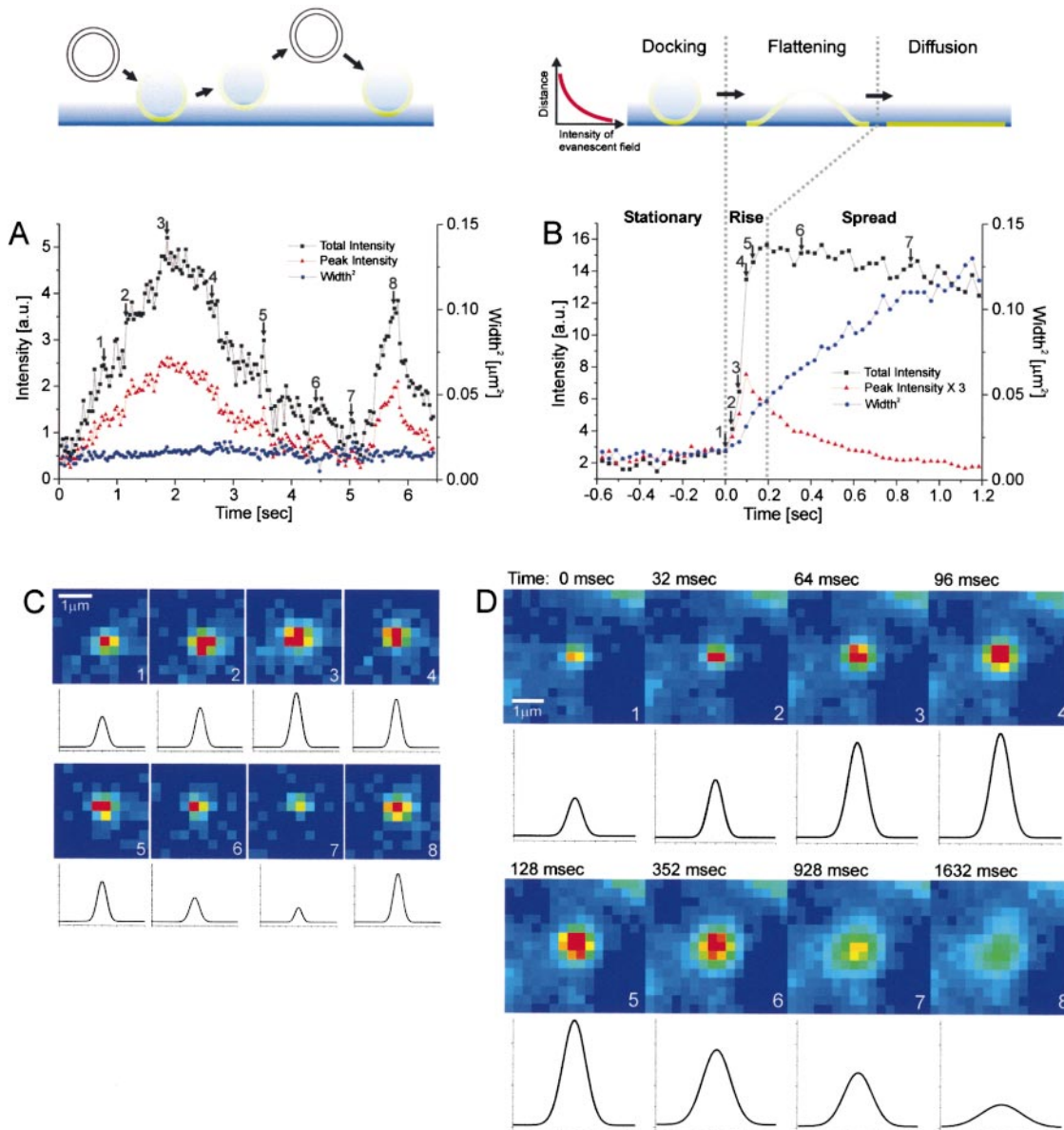


**Figure 2.** Analysis of carriers. The VSVG-GFP fluorescence was imaged for carriers close to the plasma membrane. Selected frames are shown from a sequence in (C) for a carrier which moved perpendicular to the coverslip, without fusing to the plasma membrane and in (D) for a carrier which fused to the plasma membrane. The intensity of the VSVG-GFP in frames C and D is shown in pseudocolor. Each sequence was processed with a running average in time of ( $\pm 1$  frame) and thresholded separately to aid visualization. The radially symmetric Gauss fit of the carrier fluorescence is shown below each frame. (A and B) The total intensity, peak intensity and the square of the Gaussian width for the carriers shown in C and D were plotted over time in A and B, respectively. The numbered arrows refer to the frames from sequences C and D. In B, the three phases, stationary, rise and spread, are separated by dotted lines. Times are marked relative to the start of the rise phase.

formly distributed over the membrane and using an evanescent decay length of 50–90 nm (the estimated decay length in our experiments), the calculated ratios are between 2.7 and 5.0 (see Materials and Methods). Most experimental values obtained for the ratio from events with short rise times ( $< 200$  ms) are within this range (average of 16 events =  $4.6 \pm 2.0$ ).

### Spread Phase

During the third phase, the total intensity remained rela-

tively constant, the peak intensity decreased exponentially, and the width squared increased linearly. The observation that the total intensity remained at a plateau indicates that the fluorescence within the region of interest was conserved: fluorophores were neither moving closer to or further away from the coverslip. The subsequent slow decrease of the total intensity in this phase is probably due to photobleaching (measured at  $\sim 0.1\%$  per frame) and the diffusion of VSVG-GFP out of the region used for the analysis. The exponential decay of the peak intensity together with the increase in width can be explained by the

Table I. Qualitative Summary of the Kinetic Behavior of the Characteristic Values for a Fusing Carrier

Phase	Stationary	Rise	Spread
Total intensity	Constant	↑↑	Relatively constant
Peak intensity	Constant	↑↑	↓↓
Width	Constant	↑	↑

spread of the VSVG-GFP into the plasma membrane upon fusion. If the spread of the VSV-GFP into the membrane was diffusive then the width squared should increase linearly (Crank, 1995). Potential deviations from simple diffusion would contribute nonlinear terms. The width of the fluorescence was analyzed for 28 fusion events from 7 different cells. The data could be fit to a straight line with a correlation coefficient ( $r^2$ ) that ranged from 0.96 to 0.996. Thus, our subsequent analysis assumed that the dominant behavior was diffusive (width squared increased linearly with time), yielding an average diffusion constant of  $(1.1 \pm 0.5) \times 10^{-9} \text{ cm}^2/\text{s}$ . A diffusion constant of VSVG in the plasma membrane was previously reported to be  $(3.8 \pm 1.8) \times 10^{-10} \text{ cm}^2/\text{s}$  using FRAP measurements on fluorescently labeled Fab fragments bound to VSVG (Zhang et al., 1991). There are a few possible explanations for the difference between the two values of the diffusion constant. First, the attachment of Fab fragments to the VSVG could slow down the mobility. Second, the diffusion constant may be temperature sensitive. The FRAP experiments were performed at room temperature, whereas our measurements were performed at 33–35°C. Third, the mobility of newly delivered membrane proteins may be different from those that have been resident in the membrane. Finally, the photobleaching involved in FRAP may induce changes in the membrane that slow the subsequent diffusion.

The changes in the total, peak, and width of the fluorescence intensity through each of the three phases are representative of the fusion events for those carriers that had short rise times (Fig. 2, B and D). In addition, we observed two other types of fusion events. First, a small fraction of the events with short rise times had widths that increased at a slower-than-linear rate. This may be the consequence of a variable distance between the coverslip and the plasma membrane. In certain areas, the cell membrane buckled away from the coverslip. This was seen in TIR-FM pictures of cells that were surface-labeled with a membrane marker (data not shown). A fusion event occurring

at the edge of such a buckle, therefore, would deliver at least part of its fluorescent cargo into a region of the plasma membrane that is in a weaker part of the excitation field.

Second, there were events with significantly longer rise times that were associated with tubules. The carriers in the short rise time events described above appeared as fluorescent spots close to the plasma membrane. However, in some cases, the carriers appeared as tubules moving in and out of the evanescent field, as indicated by the intensity changes along their length (Fig. 3 and Video 3 at <http://www.jcb.org/cgi/content/full/149/1/23/DC1>). The fusion of tubules to the plasma membrane was similar to the short rise time events, with stationary, rise, and spread phases. However, these tubules were different in a few characteristics. At the beginning of the rise phase, the tubules rounded up to a circular spot ( $n > 10$ ; Fig. 3, frames at  $t = 0.0$  and 0.1 s). This accounts for the drop in the width of the fluorescence at the beginning of the rise phase (Fig. 4 A). For these tubular carriers, the rise phase lasted substantially longer ( $>1$  s) than the rise phase of the short rise time carriers (compare Fig. 4 A with Figs. 2 B and 4 B). The peak fluorescence intensity was approximately the same for both types of carriers. However, the total fluorescence intensity delivered by a tubule was up to 25-fold greater. Further, the total fluorescence continued to increase even after the peak fluorescence was reached (Fig. 4 A). This suggests there was a sustained delivery of fluorescent membrane protein into the evanescent field.

Some carriers that appeared as spots also exhibited long rise times (data not shown). These may have been tubules oriented perpendicular to the membrane. Consistent with this interpretation, carriers that had long rise times also continued to increase their total fluorescence after the peak fluorescence was reached and delivered a greater total amount of fluorescence to the membrane. For one particular cell, the carriers that had a rise time of  $>1$  s represented 21% of all the events we observed ( $n = 96$ ), but they accounted for 59% of the total fluorescence intensity (Table II). This is consistent with a model in which longer rise times result from the fusion of larger carriers (tubules), deliver a larger amount of VSVG-GFP to the plasma membrane (supplementary Figure 1).

For regulated exocytosis, considerable evidence has accumulated to favor a vesicular model. Two different structures have been proposed as the carriers for constitutive exocytosis from the Golgi complex to the plasma mem-

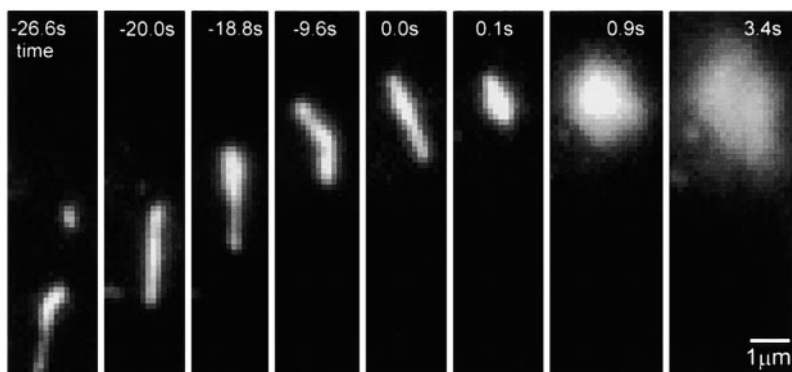
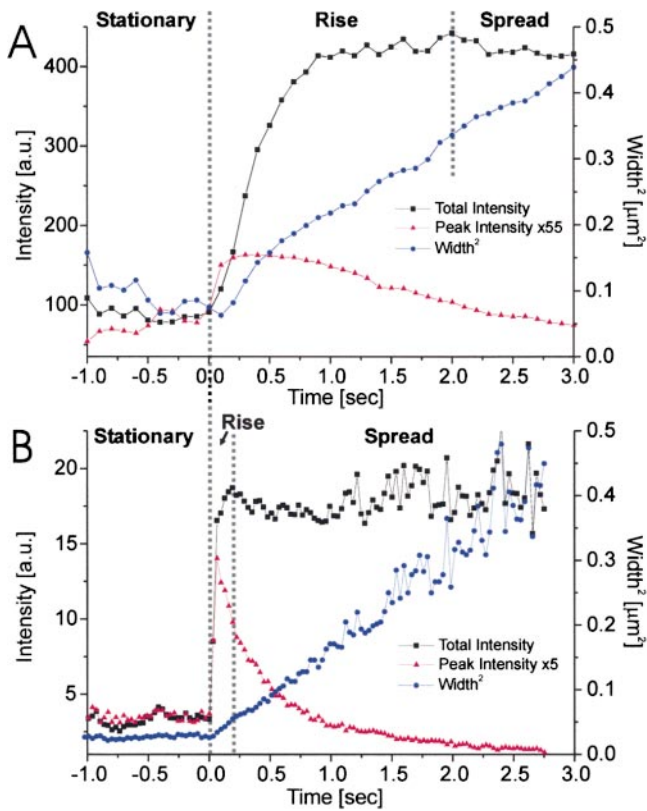


Figure 3. Selected frames from a sequence showing the transport, docking, and fusion of a tubular carrier. Times are marked relative to the start of the rise phase.



**Figure 4.** Carrier fusion events with different rise times. Total intensity, peak intensity, and square of the Gaussian width were plotted on the same time axis for carriers with long and short rise times (time is marked relative to the start of the rise phase). (A) A carrier with a long rise time ( $\sim 1.9$  s) and tubular morphology (taken from the sequence shown in Fig. 3). (B) A carrier with short rise time ( $\sim 160$  ms) and spotlike morphology. A similar example is shown in Fig. 2 D. The three phases, stationary, rise and spread, are separated by dotted lines.

brane: spherical and tubular vesicles (Hirschberg et al., 1998; Toomre et al., 1999). Our observations support the presence of both. However, rather than representing two separate classes of carriers, they describe the two extremes of what we observe as a continuum of carriers of various spherical and tubular shapes and sizes. There are some potential limitations to this analysis. First, the absolute value of the maximum total intensity cannot be accurately determined. Since the distance between the cell membrane and the coverslip varied, identical carriers fusing at different sites could give different intensities. However, the large number of events analyzed compensates for such effects.

**Table II.** Statistics of Rise Times and Total Delivered Fluorescence Intensity

Rise time	<200 ms	200 ms–1 sec	>1 sec
Percentage of total events ( $n = 130$ ), 7 cells	31	48	21
Percentage of total fluorescence intensity delivered ( $n = 96$ ), 1 cell*	11	30	59

\*Since the total fluorescence intensity delivered to the plasma membrane is difficult to compare between different experiments because of variations in the evanescent field intensities, the percentages of the total intensity are calculated from a single cell experiment (no. fusions = 96).

Second, there may have been very small carriers present, whose fusion would be undetectable because of their low fluorescence. Finally, TIR-FM is only sensitive to fusion events occurring at the cell–coverslip interface. We assume that these are representative of fusions that occur on the surface of the cell that is not in contact with the coverslip.

To check for preferred sites of fusion, we marked the coordinates of all detected fusion events ( $n = 147$ ) in a single cell over 60 min. A map of these fusion sites (red dots) was superimposed on a thresholded TIR-FM image (see Materials and Methods) of the entire field showing VSVG-GFP in the plasma membrane (Fig. 5). Since the distance between the plasma membrane and the coverslip was not uniform, there was unevenness in the plasma membrane fluorescence intensity under TIR-FM. In general, the fusion sites appear to be distributed in a fairly random manner. The areas that were devoid of fusion events colocalize well with the dark areas in the TIR-FM image. This suggests that the apparent lack of detected fusion events in these areas resulted from the membrane being further from the coverslip and, thus, not excited by the evanescent field. Alternatively, the dark areas may be inhomogeneities in the membrane that exclude VSVG-GFP and membrane fusion. In addition, we never detected repeated fusion at exactly the same coordinates. This indicates that in this system, the fusion of carriers in constitutive exocytosis occurs all over the plasma membrane and that there are no preferred sites for fusion.

Regulated secretion in nerve terminals is primarily constrained to the synaptic junction. Here, the calcium channels and secretory vesicles are maintained in close proximity. In contrast, our results indicate that there are no preferred sites for release in constitutive exocytosis. The lack of repeated exocytosis at any specific point raises questions about the biochemical requirements for constitutive exocytosis. Perhaps regulated exocytosis remains highly localized to compartmentalize the calcium transients, and thereby maximize their effect on exocytosis while minimizing their effect on the total calcium load on the cell (Simon and Llinás, 1985). Constitutive exocytosis is calcium independent (Lew and Simon, 1991; Miller and Moore, 1991), and this may free the fusion machinery to diffuse all over the surface until it engages secretory cargo, which is then released at the site of contact.

Previous assays on exocytosis have studied the formation and widening of the fusion pore and the secretion of luminal contents. TIR-FM has allowed us to observe and quantify, for the first time, the flattening of the vesicle into the plasma membrane (the rise phase), which occurs over a time scale ranging from hundreds of milliseconds to a few seconds (Table II). In contrast, the initial opening of a fusion pore in regulated exocytosis, based on electrophysiological measurements, occurs on the time scale of a few milliseconds (Spruce et al., 1990). Thus, these techniques complement each other by monitoring two different steps in the fusion process. The electrophysiological experiment measures the increase in conductance between the inside of a vesicle and the outside of the cell as the fusion pore opens, whereas the optical experiment described in this paper measures the time course of the carrier membrane flattening down.

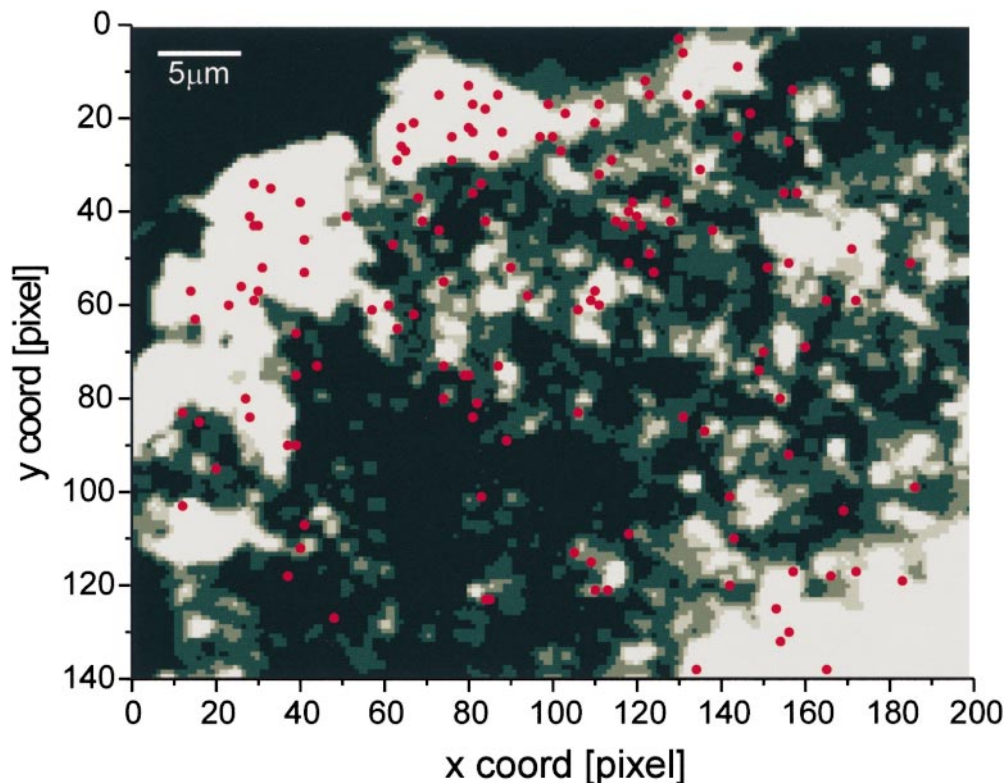


**Figure 5.** Map of fusion sites of a single cell. The exocytotic events ( $n = 147$ ) from a single cell were superimposed as red dots onto a thresholded gray scale image of VSVG-GFP in the plasma membrane (see Materials and Methods). One edge of the cell is in the upper left. Under epi-illumination, the Golgi complex appeared in the lower right corner. Pixel size, 268 nm.

The vesicular hypothesis was established by the demonstration that, in regulated exocytosis, each released quanta contains a large number of secretory molecules (Del Castillo and Katz, 1954). Using TIR-FM with a GFP-labeled membrane marker, we demonstrate that, in constitutive exocytosis, each fused quanta delivers a large number of membrane proteins to the plasma membrane. These results demonstrate that in all the events analyzed, the vesicular membrane proteins are completely delivered into the plasma membrane. In recent years, there have been a number of experiments indicating that in regulated exocytosis vesicles might only transiently fuse in what has been called kiss and run (Artalejo et al., 1998; Meldolesi, 1998; Palfrey and Artalejo, 1998; Ales et al., 1999; Fesce and Meldolesi, 1999). In this model, the vesicle forms a fusion pore that widens enough to allow the release of luminal components, but not the fusion of the vesicular membrane with the plasma membrane. Our results indicate that, in constitutive exocytosis, there are vesicles that fully fuse and integrate with the plasma membrane.

A difference in membrane tension between the vesicle and the plasma membrane has been proposed to drive the fusion of the vesicular and plasma membranes (Monck et al., 1990; Solsona et al., 1998; Markosyan et al., 1999; Siegel, 1999). The ability to quantify the rate of vesicular flattening could allow these models to be tested. One particularly intriguing observation is that the rate at which the width of the fluorescence widens is faster during the flattening of the vesicle (the rise phase of the fluorescence) than it is during the subsequent diffusion of the VSVG-GFP into the plasma membrane (the spread phase). This suggests that the VSVG-GFP is spreading into the plasma membrane at a rate faster than expected just by diffusion. With

further refinements, TIR-FM may be useful for identifying and localizing components of the fusion apparatus and elucidating the possible role of cytoskeletal and other structural elements in constitutive exocytosis. Similar results are reported for another cell line (Toomre et al., 2000).

We would like to thank Yu Chen (Rockefeller) and Yoshihiro Kawano (Olympus) for many discussions and assistance, Natalie de Souza (Rockefeller) and Yu Chen (Rockefeller) for critical reading of the manuscript, and Jennifer Lippincott-Schwartz (NIH) for the VSVG-GFP plasmid. J. Schmoranzler, M. Goulian and S.M. Simon would like to thank the Molecular Photonics Laboratory (Hamakita City, Japan) for their support.

Submitted: 13 December 1999

Revised: 18 February 2000

Accepted: 29 February 2000

#### References

- Albillos, A., G. Dernick, H. Horstmann, W. Almers, G.A. De Toledo, and M. Lindau. 1997. The exocytotic event in chromaffin cells revealed by patch amperometry. *Nature*. 389:509-512.
- Ales, E., L. Tabares, J.M. Poyato, V. Valero, M. Lindau, and D.T. Alvarez. 1999. High calcium concentrations shift the mode of exocytosis to the kiss-and-run mechanism. *Nat. Cell Biol.* 1:40-44.
- Artalejo, C.R., A. Elhamdani, and H.C. Palfrey. 1998. Secretion: dense-core vesicles can kiss-and-run too. *Curr. Biol.* 8:R62-R65.
- Axelrod, D. 1989. Total internal reflection fluorescence microscopy. *Methods Cell Biol.* 30:245-270.
- Axelrod, D., E.H. Hellen, and R.M. Fulbright. 1992. Total internal reflection fluorescence. In *Topics in Fluorescence Spectroscopy, Volume 3: Biochemical Applications*. J.R. Lakowicz, editor. Plenum Press, New York. 289-343.
- Crank, J. 1975. *The Mathematics of Diffusion*. Oxford University Press.
- Del Castillo, J., and B. Katz. 1954. Quantal components of the end-plate potential. *J. Physiol.* 124:560-573.
- Fatt, P., and B. Katz. 1952. Spontaneous subthreshold activity at motor nerve endings. *J. Physiol.* 117:109-128.
- Fernandez, J.M., E. Neher, and B.D. Gomperts. 1984. Capacitance measurements reveal stepwise fusion events in degranulating mast cells. *Nature*. 312: 453-455.
- Fesce, R., and J. Meldolesi. 1999. Peeping at the vesicle kiss. *Nat. Cell Biol.*

- 1:E3–E4.
- Funatsu, T., Y. Harada, M. Tokunaga, K. Saito, and T. Yanagida. 1995. Imaging of single fluorescent molecules and individual ATP turnovers by single myosin molecules in aqueous solution. *Nature*. 374:555–559.
- Gillis, K.D., R.Y. Pun, and S. Mislser. 1991. Single cell assay of exocytosis from adrenal chromaffin cells using “perforated patch recording.” *Pflugers Arch*. 418:611–613.
- Hirschberg, K., C.M. Miller, J. Ellenberg, J.F. Presley, E.D. Siggia, R.D. Phair, and J. Lippincott-Schwartz. 1998. Kinetic analysis of secretory protein traffic and characterization of golgi to plasma membrane transport intermediates in living cells. *J. Cell Biol*. 143:1485–1503.
- Inoué, S., and K.R. Spring. 1997. *Video Microscopy: The Fundamentals*. Plenum Press, New York. 765 pp.
- Lang, T., I. Wacker, J. Steyer, C. Kaether, I. Wunderlich, T. Soldati, H.H. Gerdes, and W. Almers. 1997. Ca<sup>2+</sup>-triggered peptide secretion in single cells imaged with green fluorescent protein and evanescent-wave microscopy. *Neuron*. 18:857–863.
- Lew, D.J., and S.M. Simon. 1991. Characterization of constitutive exocytosis in the yeast *Saccharomyces cerevisiae*. *J. Membr. Biol*. 123:261–268.
- Markosyan, R.M., G.B. Melikyan, and F.S. Cohen. 1999. Tension of membranes expressing the hemagglutinin of influenza virus inhibits fusion. *Biophys. J*. 77:943–952.
- Meldolesi, J. 1998. Regulated exocytosis in neurons and neurosecretory cells: structural events and expression competence. *J. Physiol*. 92:119–121.
- Migler, K., and H.L.L. Hervet. 1993. Slip transition of a polymer melt under shear-stress. *Phys. Rev. Lett*. 70:287–290.
- Miller, S.G., and H.-P. Moore. 1991. Reconstitution of constitutive secretion using semi-intact cells: regulation by GTP but not calcium. *J. Cell Biol*. 112:39–54.
- Monck, J.R., D.T. Alvarez, and J.M. Fernandez. 1990. Tension in secretory granule membranes causes extensive membrane transfer through the exocytotic fusion pore. *Proc. Natl. Acad. Sci. USA*. 87:7804–7808.
- Neher, E., and A. Marty. 1982. Discrete changes of cell membrane capacitance observed under conditions of enhanced secretion in bovine adrenal chromaffin cells. *Proc. Natl. Acad. Sci. USA*. 79:6712–6716.
- Nusse, O., and M. Lindau. 1988. The dynamics of exocytosis in human neutrophils. *J. Cell Biol*. 107:2117–2123.
- Oheim, M., D. Loerke, W. Stühmer, and R.H. Chow. 1998. The last few milliseconds in the life of a secretory granule. Docking, dynamics and fusion visualized by total internal reflection fluorescence microscopy (TIRFM). *Eur. Biophys. J. Biophys. Lett*. 27:83–98.
- Palade, G.E. 1975. Intracellular aspects of the process of protein secretion. *Science*. 189:347–358.
- Palfrey, H.C., and C.R. Artalejo. 1998. Vesicle recycling revisited: rapid endocytosis may be the first step. *Neuroscience*. 83:969–989.
- Presley, J.F., N.B. Cole, T.A. Schroer, K. Hirschberg, K.J. Zaal, and J. Lippincott-Schwartz. 1997. ER-to-Golgi transport visualized in living cells. *Nature*. 389:81–85.
- Rothman, J.E., and F.T. Wieland. 1996. Protein sorting by transport vesicles. *Science*. 272:227–234.
- Ryan, T.A., H. Reuter, and S.J. Smith. 1997. Optical detection of a quantal presynaptic membrane turnover. *Nature*. 388:478–482.
- Siegel, D.P. 1999. The modified stalk mechanism of lamellar/inverted phase transitions and its implications for membrane fusion. *Biophys. J*. 76:291–313.
- Simon, S.M., and R.R. Llinás. 1985. Compartmentalization of the submembrane calcium activity during calcium influx and its significance in transmitter release. *Biophys. J*. 48:485–498.
- Solsona, C., B. Innocenti, and J.M. Fernandez. 1998. Regulation of exocytotic fusion by cell inflation. *Biophys. J*. 74:1061–1073.
- Spruce, A.E., L.J. Breckenridge, A.K. Lee, and W. Almers. 1990. Properties of the fusion pore that forms during exocytosis of a mast cell secretory vesicle. *Neuron*. 4:643–654.
- Steyer, J.A., H. Horstmann, and W. Almers. 1997. Transport, docking and exocytosis of single secretory granules in live chromaffin cells. *Nature*. 388:474–478.
- Toomre, D., P. Keller, J. White, J.C. Olivo, and K. Simons. 1999. Dual-color visualization of trans-Golgi network to plasma membrane traffic along microtubules in living cells. *J. Cell Sci*. 112:21–33.
- Toomre, D., J.A. Steyer, P. Keller, W. Almers, and K. Simons. 2000. Fusion of constitutive membrane traffic with the cell surface observed by evanescent wave microscopy. *J. Cell Biol*. 149:33–40.
- Wehland, J., M.C. Willingham, M.G. Gallo, and I. Pastan. 1982. The morphologic pathway of exocytosis of the vesicular stomatitis virus G protein in cultured fibroblasts. *Cell*. 28:831–841.
- Zhang, F., B. Crise, B. Su, Y. Hou, J.K. Rose, A. Bothwell, and K. Jacobson. 1991. Lateral diffusion of membrane-spanning and glycosylphosphatidylinositol-linked proteins: towards establishing rules governing the lateral mobility of membrane proteins. *J. Cell Biol*. 115:75–84.
- Zhou, Z., and S. Mislser. 1995. Amperometric detection of stimulus-induced quantal release of catecholamines from cultured superior cervical ganglion neurons. *Proc. Natl. Acad. Sci. USA*. 92:6938–6942.
- Zimmerberg, J., M. Curran, F.S. Cohen, and M. Brodwick. 1987. Simultaneous electrical and optical measurements show that membrane fusion precedes secretory granule swelling during exocytosis of beige mouse mast cells. *Proc. Natl. Acad. Sci. USA*. 84:1585–1589.
- Zimmerberg, J., R. Blumenthal, D.P. Sarkar, M. Curran, and S.J. Morris. 1994. Restricted movement of lipid and aqueous dyes through pores formed by influenza hemagglutinin during cell fusion. *J. Cell Biol*. 127:1885–1894.